20030108161

PHYSICAL MODELING TECHNIQUES FOR MISSILE
AND OTHER
PROTECTIVE STRUCTURES

Papers Submitted for Presentation During the
American Society of Civil Engineers
National Spring Convention
Las Vegas, April 1982

Sponsored By the ASCE Engineering Mechanics Division
Committee on Experimental Analysis and Instrumentation

Edited By: T. Krauthammer and C. D. Sutton

REPLY TO
ATTN OF   PA   29 Jun 83

SUBJECT   Review of Material for Public Release

TO   Mr. James Shafer
          Defense Technical Information Center
          DDAC
          Cameron Station
          Alexandria, VA 22314

          The following technical papers have been reviewed by our office and are
          approved for public release. This headquarters has no objection to their
          public release and authorizes publication.

          1. (BMO 81-296) "Protective Vertical Shelters" by Ian Narain, A.M. ASCE,
          Jerry Stepheno, A.M. ASCE, and Gary Landon, A.M. ASCE.

          2. (BMO 82-020) "Dynamic Cylinder Test Program" by Jerry Stephens, A.M.
          ASCE.

          3. (AFCMD/82-018) "Blast and Shock Field Test Management" by Michael
          Noble.

          4. (AFCMD/82-014) "A Comparison of Nuclear Simulation Techniques on
          Generic MX Structures" by John Betz.

          5. (AFCMD/82-013) "Finite Element Dynamic Analysis of the DCT-2 Models"
          by Barry Bingham.

          6. (AFCMD/82-017) "MX Basing Development Derived From H. E. Testing" by
          Donald Cole.

          7. (BMO 82-017) "Testing of Reduced-Scale Concrete MX-Shelters-
          Experimental Program" by J. I. Daniel and D. M. Schultz.

          8. (BMO 82-017) "Testing of Reduced-Scale Concrete MX-Shelters-Specimen
          Construction" by A. T. Ciolko.

          9. (BMO 82-017) "Testing of Reduced-Scale Concrete MX-Shelters-
          Instrumentation and Load Control" by N. W. Hanson and J. T. Julien.

          10. (BMO 82-003) "Laboratory Investigation of Expansion, Venting, and
          Shock Attenuation in the MX Trench" by J. K. Gran, J. W. Bruce, and J. D.
          Colton.

11. (BMO 82-003) "Small-Scale Tests of MX Vertical Shelter Structures" by J. K. Gran, J. R. Bruce, and J. D. Colton.

12. (BMO 82-001) "Determination of Soil Properties Through Ground Motion Analysis" by John Frye and Norman Lipner.

13. (BMO 82-062) "Instrumentation for Protective Structures Testing" by Joe Quintana.

14. (BMO 82-105) "1/5 Size VHS Series Blast and Shock Simulations" by Michael Noble.

15. (BMO 82-126) "The Use of Physical Models in Development of the MX Protective Shelter" by Eugene Sevin.

*16. REJECTED: (BMO 82-029) "Survey of Experimental Work on the Dynamic Behavior of Concrete Structures in the USSR" by Leonid Millstein and Gajanen Sabnis.

CAROL A. SCHALKHAM, 1Lt, USAF
Public Affairs Officer

Cy To: Dr. T. Krauthammer
        Associate Professor
        Department of Civil and
        Mineral Engineering
        University of Minnesota

LABORATORY INVESTIGATION OF EXPANSION, VENTING,
AND SHOCK ATTENUATION IN THE MX TRENCH[1,2]

James K. Gran,[*] John R. Bruce,[*] and James D. Colton[†]

Abstract

An experimental program using 1/26-scale models of a buried
concrete trench was conducted to study the dynamics of expansion and
venting caused by an airblast propagating down the trench, and to study
the effects of the expansion and venting on the attenuation of the
airblast. The trench models were made of steel fiber-reinforced
concrete and were buried in sand. The airblast was produced with an
explosively driven shock tube. Expansion and venting dynamics of short
trench sections were studied for flat-topped pressure pulses ranging
from 700 psi to 2600 psi. Radial expansion histories and vent-times
were recorded. Shock attenuation was studied with 60-ft-long trenches
in which the peak pressure of an exponential waveform decreased from
4000 psi to 300 psi as the shock propagated the length of the trench.
The effects of expansion were isolated by comparing the attenuation in a
concrete trench to that in a steel trench. Expansion reduced the peak
pressure slightly at distances greater than 40 ft. The data were used
to validate computer models for shock attenuation in the MX trench.

Introduction

An important aspect of the MX trench is its response to air shock
waves created inside the trench. The objectives of the work presented
here were twofold: (1) to determine the expansion and venting response
of the trench under internal pressure loading and (2) to determine the
effects of attenuation mechanisms (viscous wall drag, trench expansion,
and trench-to-surface venting) on the air shock wave inside the trench.

---

[*]Research Engineer, SRI International

[†]Director of Engineering Mechanics Department, SRI International

Expansion and Venting Tests

Experimental Setup

The expansion and venting tests were conducted with the assembly shown in Fig. 1. The trench is subjected to the largest internal pressure when the shock wave produced by the explosive has traversed the run-up section and the model, and reflects from the reflecting wall at the end of the model. The assembly rested in a soil bin that provided two feet of soil to each side and below the model trench. Pressure was measured in the shock tube run-up section and at the reflecting wall. Response was photographed with two high-speed cameras, one viewing the end of the trench through the Lucite window, the other viewing the soil surface from the side.
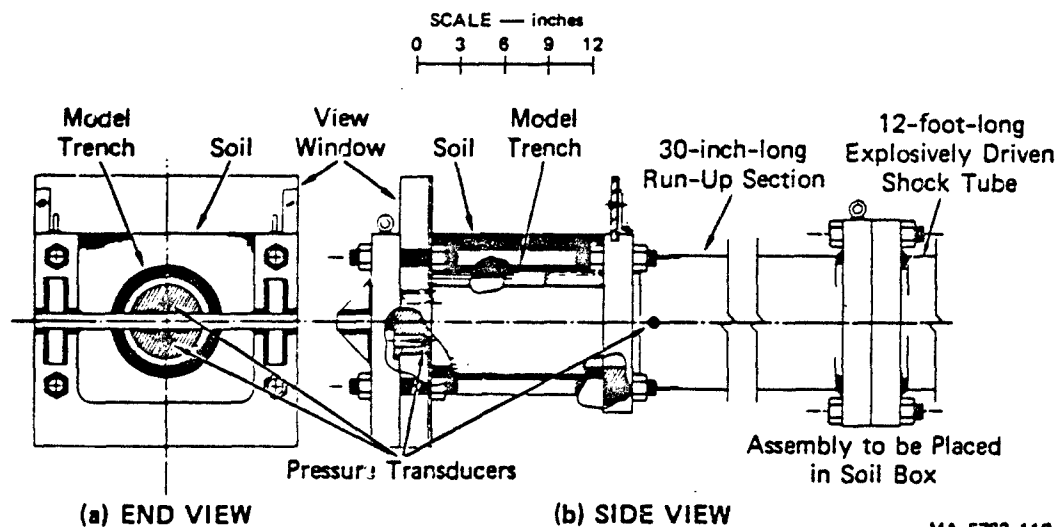

FIGURE 1 EXPANSION AND VENTING EXPERIMENT ASSEMBLY

Eight strands of explosive cord in the shock tube were used to generate nominally flat-topped shock waves with reflected pressures ranging from about 700 psi to about 2600 psi. These loads were calibrated with a steel tube in place of the model trench. The calibration pressure records are shown in Fig. 2.

2

(a) TEST 12   (b) TEST 13   (c) TEST 14
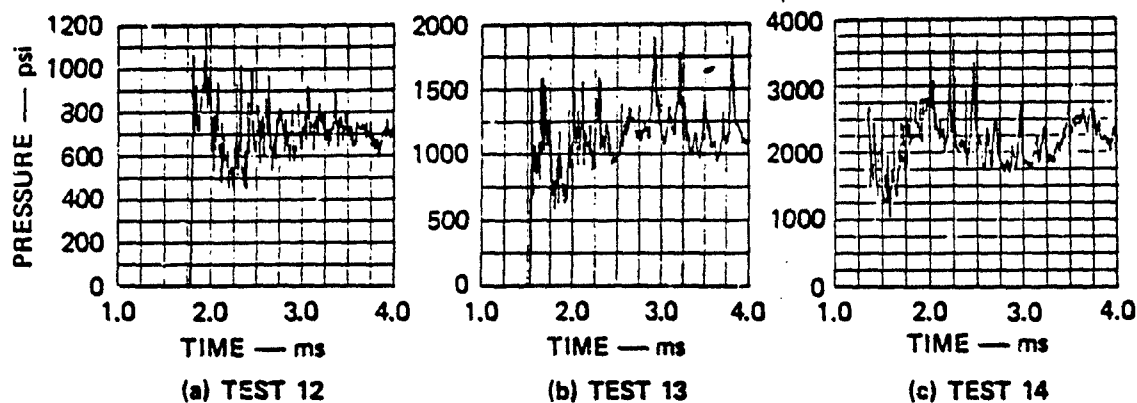
MA-6307-104

FIGURE 2   PRESSURE MEASURED AT THE REFLECTING WALL IN THE SHOCK TUBE
CALIBRATION TESTS

The expansion and venting tests were performed using 6-in.-ID,
12-in.-long trench models having a wall thickness of 0.75 in. Two
longitudinal 0.56-in.-deep saw cuts offset 110 degrees from each other
and two transverse 0.56-in.-deep saw cuts at the third points separated
the roof blocks. A typical trench model is shown in Fig. 3.
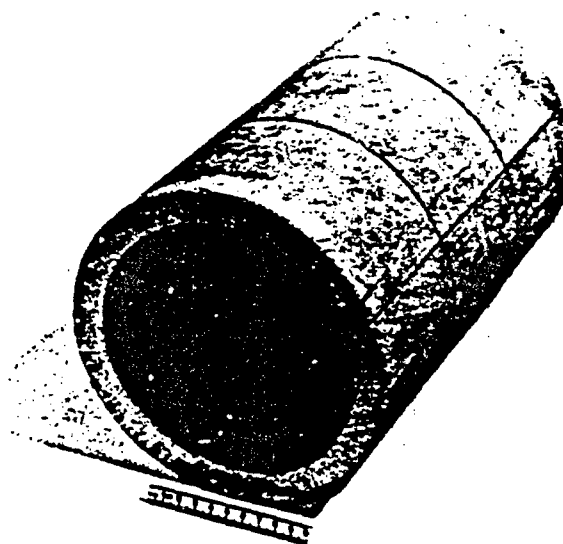
MP-6307-61

FIGURE 3   FIBER-REINFORCED CONCRETE TRENCH MODEL
WITH SAW-CUT ROOF BLOCKS

3

The formula used for the fiber-reinforced concrete was similar to that used by the Air Force Weapons Laboratory (AFWL) in the fabrication of 1/2-scale trench models. The steel fibers are U.S. Steel Fibercon, 0.010 in. in diameter and 0.5 in. long. They represent about 1.7% of the concrete mix by weight (0.5% by volume). Eight unconfined compression tests (ASTM C39-64) and 5 split-cylinder tension tests (ASTM C496-71) were performed on 3-in.-diameter, 6-in.-long samples.[3] The compression strength varied from 6590 psi to 8420 psi and averaged 7430 psi. The split-cylinder tension strength varied from 820 psi to 1010 psi and averaged 900 psi.

The soil used in the expansion and venting experiments was obtained from a designated location at the HAVE HOST test site on the Luke Air Force Range in Arizona where AFWL's 1/2-scale tests were performed. The soil was packed around the model trench manually, and samples were taken to measure the soil density and moisture content. Densities (except Test 20, the dry soil test) ranged from 117 to 122 lb/ft^3 with moisture contents from 2.6 to 3.9%. The soil cover depth was 2.3 in.

Experimental Results

Many expansion and venting experiments were conducted. Only five are described in this paper. The parameters of these experiments are given in Table 1.

Table 1

TEST PARAMETER FOR EXPANSION AND VENTING TESTS

Parameter	Test Number				
	17	18	19	20	22
Soil density	122	122	122	120-122	118
Moisture content	3.3	2.6	2.8	0.3-1.9	3.6
Peak pressure	700	1100	1100	1100	2600

The following general features were observed in this set of experiments:

(1) Several longitudinal cracks form in a circumferentially symmetric distribution in the trench wall almost immediately (within 0.3 ms) after the arrival of the shock wave. Fig. 4 shows the cracking patterns observed in Test 17 and Fig. 5(a) shows the recovered trench fragments. Fig. 5(b) shows the crack pattern observed in an AFWL 1/2-scale test. The patterns are the same for both scales.
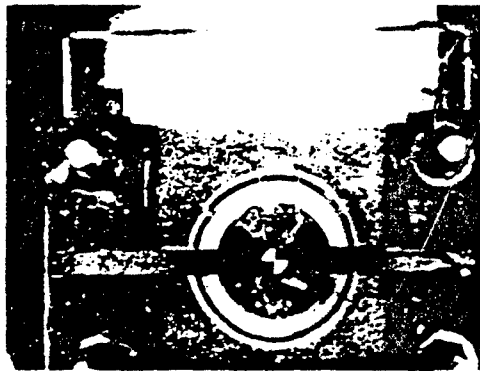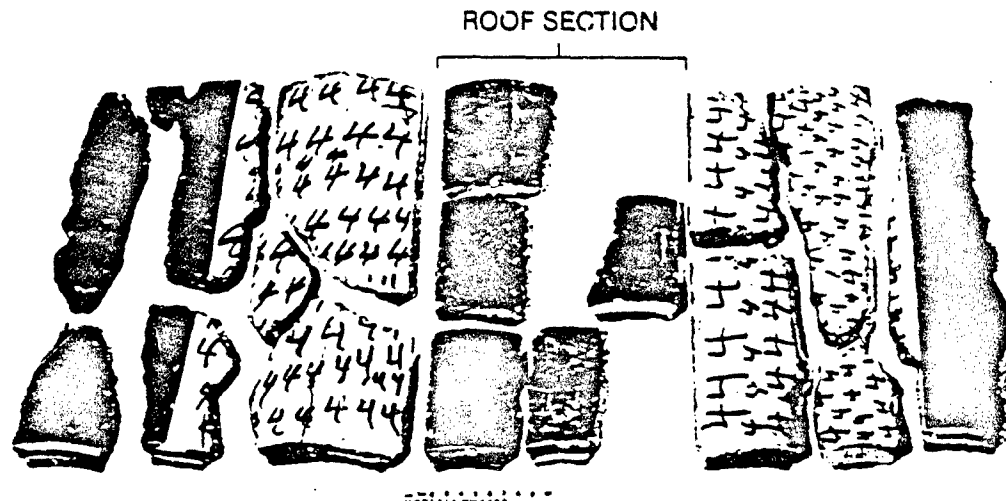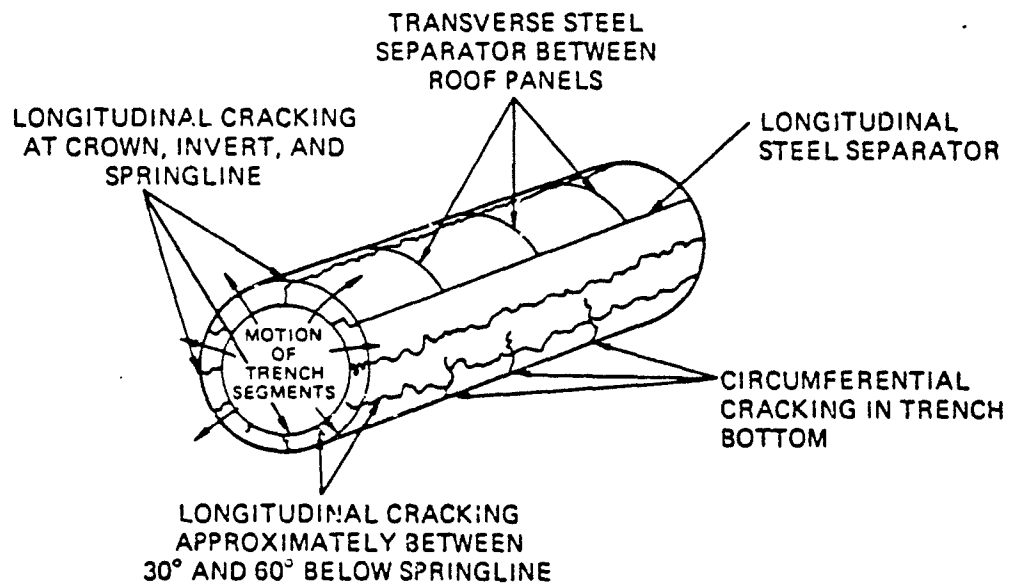

(t = 2.20 ms, Test 17)

MP-6307-15B

FIGURE 4   TRENCH CRACKING PATTERN

(2) The expansion of the trench into the soil is cylindrically symmetric until the rarefaction wave returns from the free soil surface to the trench roof. Fig. 6 illustrates this phenomenon as observed in Test 17. In this illustration, the shock wave arrives at the reflecting wall at 1.7 ms, and the trench begins to expand symmetrically. Based on a soil wave speed of 465 ft/s (observed in a previous test), the pressure wave in the soil reaches the surface about 0.45 ms later, after which the soil surface begins to move. After another 0.45 ms, the relief wave from the soil surface reaches the crown, ending the symmetric phase of the expansion.

5

ROOF SECTION

(a) RECOVERED TRENCH FRAGMENTS FROM SRI TEST 17 (1/26-Scale)

TRANSVERSE STEEL
SEPARATOR BETWEEN
ROOF PANELS

LONGITUDINAL CRACKING
AT CROWN, INVERT, AND
SPRINGLINE

LONGITUDINAL
STEEL SEPARATOR

MOTION
OF
TRENCH
SEGMENTS

CIRCUMFERENTIAL
CRACKING IN TRENCH
BOTTOM

LONGITUDINAL CRACKING
APPROXIMATELY BETWEEN
30° AND 60° BELOW SPRINGLINE

(b) CRACK PATTERN OBSERVED IN AFWL 1/2-SCALE TEST T-1

MP-6307-17B

FIGURE 5   COMPARISON OF TRENCH CRACK PATTERNS BETWEEN SRI 1/26-SCALE TESTS
AND AFWL 1/2-SCALE TEST T-1

6
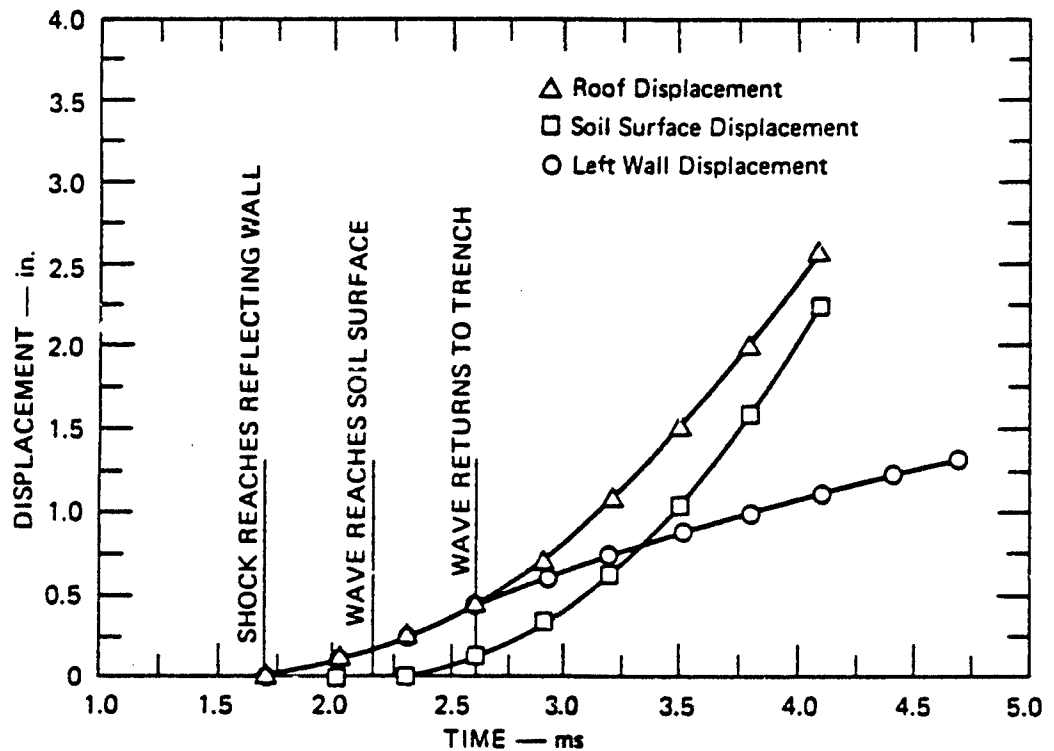
FIGURE 6   SYMMETRIC TRENCH EXPANSION PHASE (Test 17)

(3)   After the symmetric expansion phase, the slug of roof
      fragments moves vertically with little or no change of
      shape until venting occurs. The soil above the crown
      mounds up without much lateral flow. The expansion of
      the trench at the springlines and floor continues to be
      approximately symmetric. Fig. 7 illustrates this phase
      of expansion in Test 17.

(4)   Venting begins at the roof crack nearest the crown, when
      the trench roof has moved to about the level of the
      original soil surface. Initiation of venting in Test 17
      is shown in Fig. 8.

7
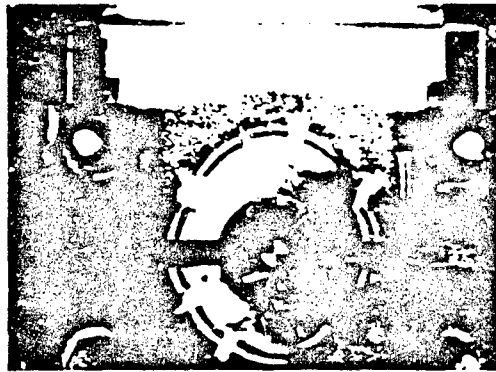
(t = 3.70 ms, Test 17)   (t = 4.20 ms, Test 17)

MP-6307-15C   MP-6307-15D

FIGURE 7   ASYMMETRIC EXPANSION PHASE   FIGURE 8   INITIATION OF VENTING AT
   CRACK NEAREST CROWN

(5)   Once venting begins (near the reflecting wall), the soil
       surface unzips along the length of the trench at about
       the same rate as the propagation of the reflected shock
       wave. This phenomenon as observed in Test 17, is illus-
       trated in Fig. 9. (The unzipping phenomenon was
       difficult to observe with short test sections, espe-
       cially at the higher pressures, but the shock attenua-
       tion tests with long trenchs verified this response
       feature.)
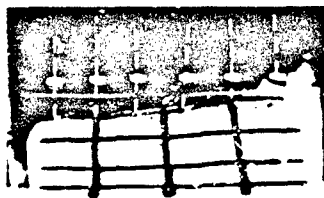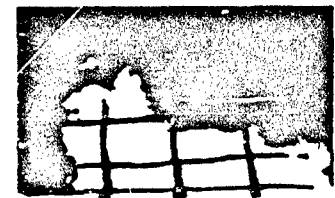
(a) t = 4.10 ms   (b) t = 4.50 ms   (c) t = 4.95 ms

MP-6307-16C

FIGURE 9   SIDE VIEW OF GROUND SURFACE ABOVE THE TRENCH MODEL
(Photo pins used to measure absolute roof displacement)

8

The effect of pressure on venting is illustrated in Fig. 10, where the time of venting and the roof displacement at the time of venting are plotted against pressure. For this series of tests, a higher pressure caused venting to occur sooner and with less roof displacement. The lines drawn through the data are not fitted curves; they indicate only the trend. The data from Tests 18 and 19 do not lie near the lines. Even though in Tests 18 and 19 several measurements were repeatable, the venting data from these tests are considered anomalous because premature venting initiated through a path provided by a photo pin positioned to provide data on the motion of the trench roof.
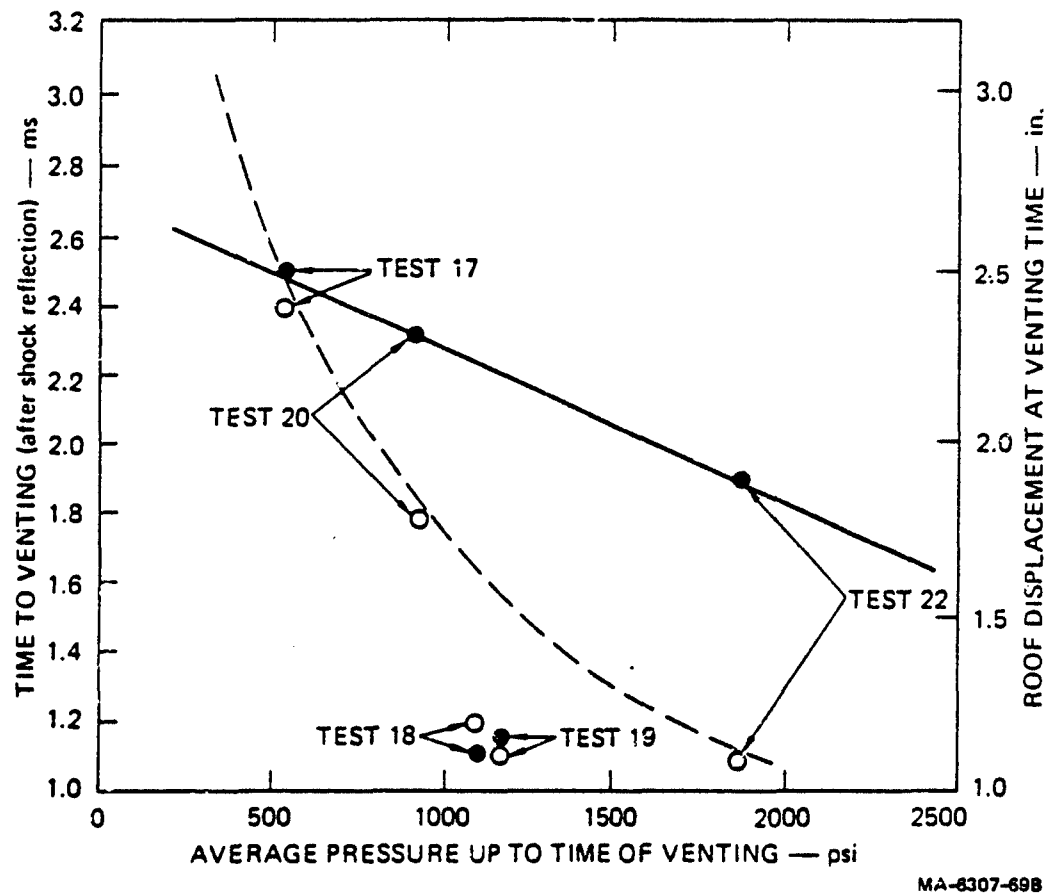

MA-6307-69B

FIGURE 10   EFFECT OF PRESSURE ON VENTING TIME AND ROOF DISPLACEMENT
AT VENTING TIME FOR REINFORCED CONCRETE TRENCHES

(O — venting time, ● — roof displacement)

9

The effect of pressure on trench fragmentation is illustrated in Table 2, which lists the number of longitudinal cracks seen in the reinforced concrete trench models at various pressures. These data suggest that slightly more cracking occurs at higher pressures; however more data is needed to substantiate this possibility.

Table 2
EFFECT OF PRESSURE ON LONGITUDINAL CRACKING

Test Number	Nominal Peak Pressure	Number of Cracks
17	700	8
18	1100	10
19	1100	9
20	1100	7
22	2600	12

Analysis of Experimental Data

To assure the consistency of the data, we performed some basic analyses, in which we treated response features separately and did not attempt to calculate the entire response in a single analysis. The response features analyzed were:

(1) Roof motion calculated from the pressure measured at the reflecting wall.

(2) Trench expansion at the springlines and invert calculated from the pressure measured at the reflecting wall.

The motion of the roof was calculated to verify the consistency of the pressure measurements and the roof displacement measurements. A one-dimensional model was adequate to calculate the displacement of the roof up to the original soil surface level.

The mathematical model used to predict the roof displacement consists of an infinitesimal ring element of roof material and cover soil

10

loaded by internal pressure. Inertial effects are dominant over the
effects of material strength, therefore, material strength was neg-
lected. The roof/soil ring element was assumed to have a constant mass.
A kinematic constraint (consistent with observation) required the thick-
ness of the ring element to remain constant. Thus, as the inside radius
grows, the loaded area increases and the mass density of the ring
element decreases. The equation of motion for this model is

$$Pa \ (d\theta) = \rho \ \frac{(b^2-a^2)}{2} \ \frac{d^2}{dt^2} \ (a+b)/2$$

where P is the pressure, a is the inside radius, b is the outside
radius, and ρ is the mass density of the ring. The assumptions of
constant mass and constant thickness reduce this equation to

$$2\pi \ Pa = m \ \frac{d^2a}{dt^2}$$

where m is the mass per unit length of a full ring.

This model was used to calculate the roof displacement for each of
the expansion and venting tests. Figure 11 compares the results of the
calculations with roof displacement measurements taken from the films
for tests with peak reflected pressures of 700 psi (Test 17), 1100 psi
(Test 18), and 2600 psi (Test 22). The soil displacement for Test 17 is
also given, indicating that about 0.4 in. of compression occurred in the
soil cover. The correlation of the calculations with the data enhances
the reliability of the pressure and displacement measurements and
indicates that the simple model for predicting roof motion is adequate.

The trench expansion into the surrounding soil was calculated to
verify the consistency of the pressure and displacement data, and also
to confirm the soil wave speed observed in the high-speed movies. The
problem was formulated for an axisymmetric, plane strain analysis.
Calculations were made with SRI PUFF, a finite difference computer code
capable of analyzing two-dimensional continua undergoing large
deformation.[5]
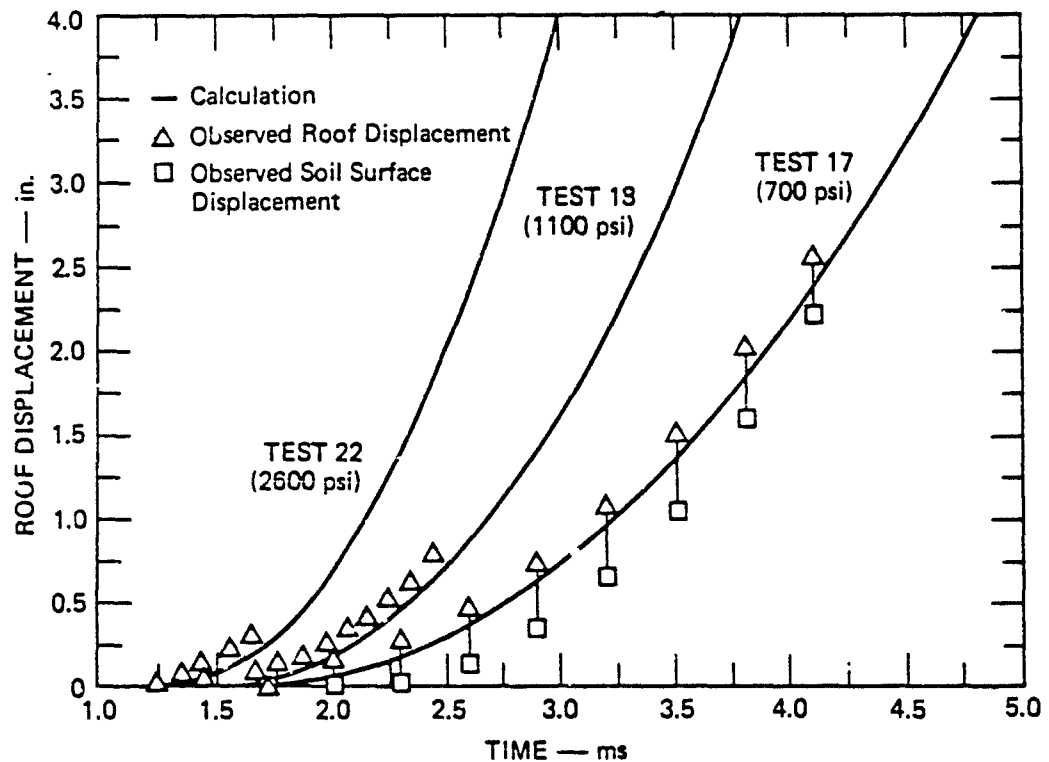
FIGURE 11   COMPARISON OF CALCULATED AND MEASURED ROOF DISPLACEMENT

The trench wall was modeled with typical concrete properties, allowing fracture at a low tensile stress. The radial compressive deformation of the concrete is negligible compared with the radial displacement. The soil was modeled as a Mohr-Coulomb material without dilatancy due to shear. In this model, the dilatational response is governed only by a variable bulk modulus (K). The distortional response is governed by two parameters, the cohesion c and the friction angle ϕ.

The soil properties were determined from the U.S. Army Waterways Experiment Station's (WES) uniaxial strain test data on HAVE HOST backfill.[4] In the calculations, the loading pressure-volume path was made to follow the $\sigma_z - \varepsilon_z$ curves given in Ref. 4. For unloading, a bulk modulus equal to the maximum loading modulus was used. A good

12

correlation with the expansion test data was obtained using soil parameters computed from WES's lower bound curve for low density soil even though our measured wet soil density was 5% to 10% higher than WES's low density soil.

One reason for using the lower bound low density stress-strain curve is that the bulk modulus computed from that curve, up to about 4% vertical strain, agrees with the bulk modulus estimated from our observed wave speed. Also, we calculated the trench expansion due to the pressure measured in Test 17 (700 psi nominal) using both the lower bound low density soil data and the upper bound high density soil data. The values of c and φ were taken directly from the WES data. The results of these two calculations are shown in Fig. 12, along with the Test 17 results. Clearly, the low density soil data produce a more accurate expansion calculation.
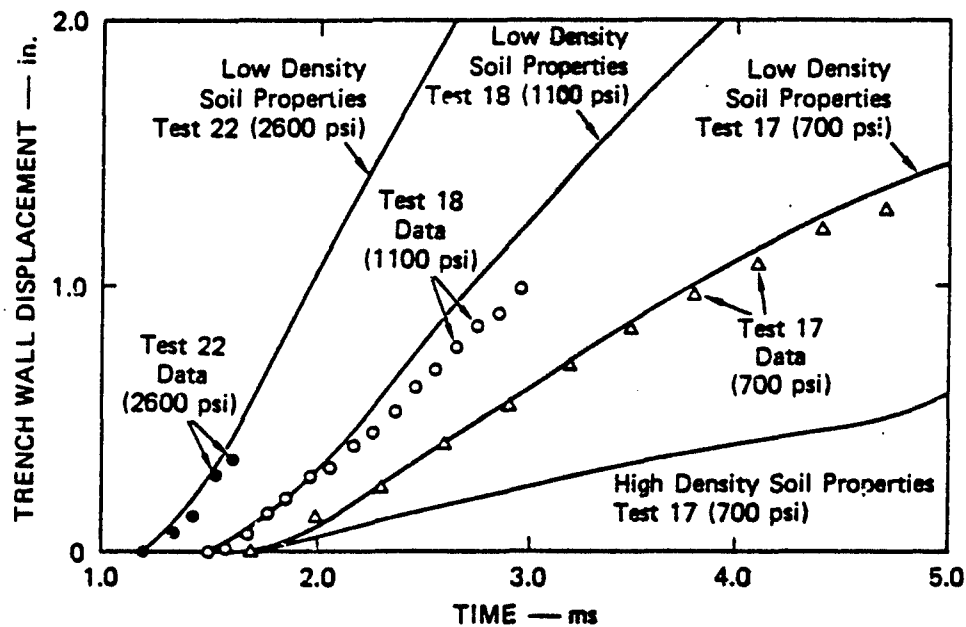

MA-6307-66

FIGURE 12   COMPARISON OF CALCULATED AND MEASURED SPRINGLINE
AND INVERT DISPLACEMENTS

13

We then calculated the wall motion using the pressures measured in Test 18 (1100 psi nominal) and Test 22 (2600 psi nominal) with the low density soil data. These calculations are also compared with the experimental results in Fig. 12. Again, the calculations and the experiments correlate well enough to confirm the reliability of the pressure and expansion data and indicate that the computational model is adequate.

Shock Attenuation Tests

Experimental Setup

The shock attenuation tests were conducted using the assembly shown in Fig. 13. A 1-in.-thick pad of COMP B was used as the explosive because of its well-characterized equation of state. To achieve a nearly plane wave, we detonated the COMP B pad simultaneously at nineteen points spaced as uniformly as possible over the back surface of the pad.
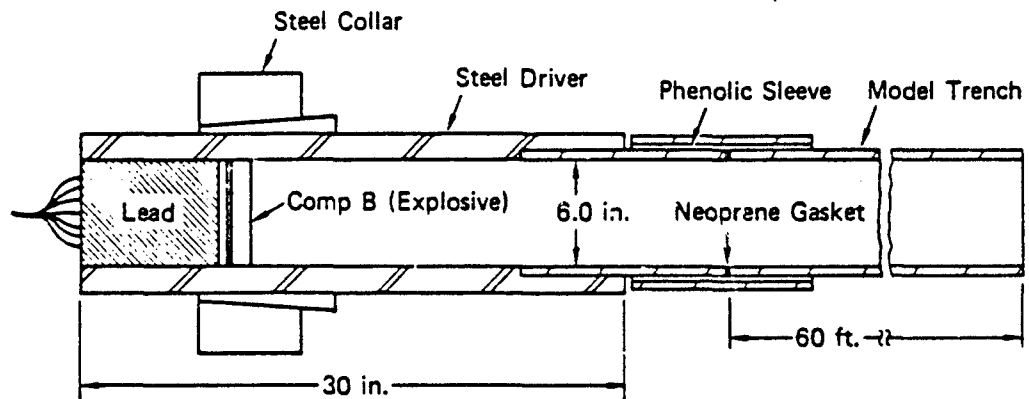
MA-7285-1A

FIGURE 13   SHOCK TUBE DRIVER CONFIGURATION

The relative effects of the various attenuation mechanisms were determined by measuring shock attenuation in a steel pipe, a deep-buried fiber-reinforced concrete trench, and a shallow-buried fiber-reinforced concrete trench, each having a length of 60 ft (120 diameters).

14

Shock pressure in the trench was measured with pressure gages in
the wall of the trench (grout was used to place the gages in the con-
crete trenches). The gage configuration had an average density approx-
imating that of the trench so that the gages would move with the trench
wall. The time of arrival (TOA) of transition zone between shocked air
and the detonation products was also measured with custom-made ioniza-
tion probes which were sensitive to the electrical conductivity of the
gas in the tube.

Steel Pipe Experiment

In the first shock attenuation test, the concrete trench was re-
placed by a steel pipe. This test defined the shock attenuation due to
frictional drag on the walls of the pipe and due to rarefactions origi-
nating upstream because of the finite thickness of the explosive charge.
The pressure records are shown in Fig. 14. The peak pressure decreased
from about 4000 psi near the source to about 700 psi near the open end
of the pipe.

To check the pressure data, we calculated peak pressures from TOA
data and compared them with the measured peak pressure. Shock velocity
at each station was obtained by fitting a polynomial to the TOA data and
differentiating this polynomial with respect to time. A fourth-degree
polynomial gave the best fit. Based on the equations for conservation
of mass and momentum, the relationship between shock velocity and
pressure is

$$P_1 - P_0 = \frac{2}{\gamma + 1} \frac{U^2}{v_o}$$

where v is specific volume, U is shock velocity, γ is the ratio of
specific heats, and P is the pressure. The subscript o refers to
conditions ahead of the shock front; the subscript 1 refers to
conditions behind the shock front.

This equation was then used to calculate the peak gage pressure
$P_1 - P_0$ at each station. For the shocked air, we used values of γ ranging
from $\gamma = 1.22$ at a pressure of 4500 psi to $\gamma = 1.38$ at 300 psi. The

15
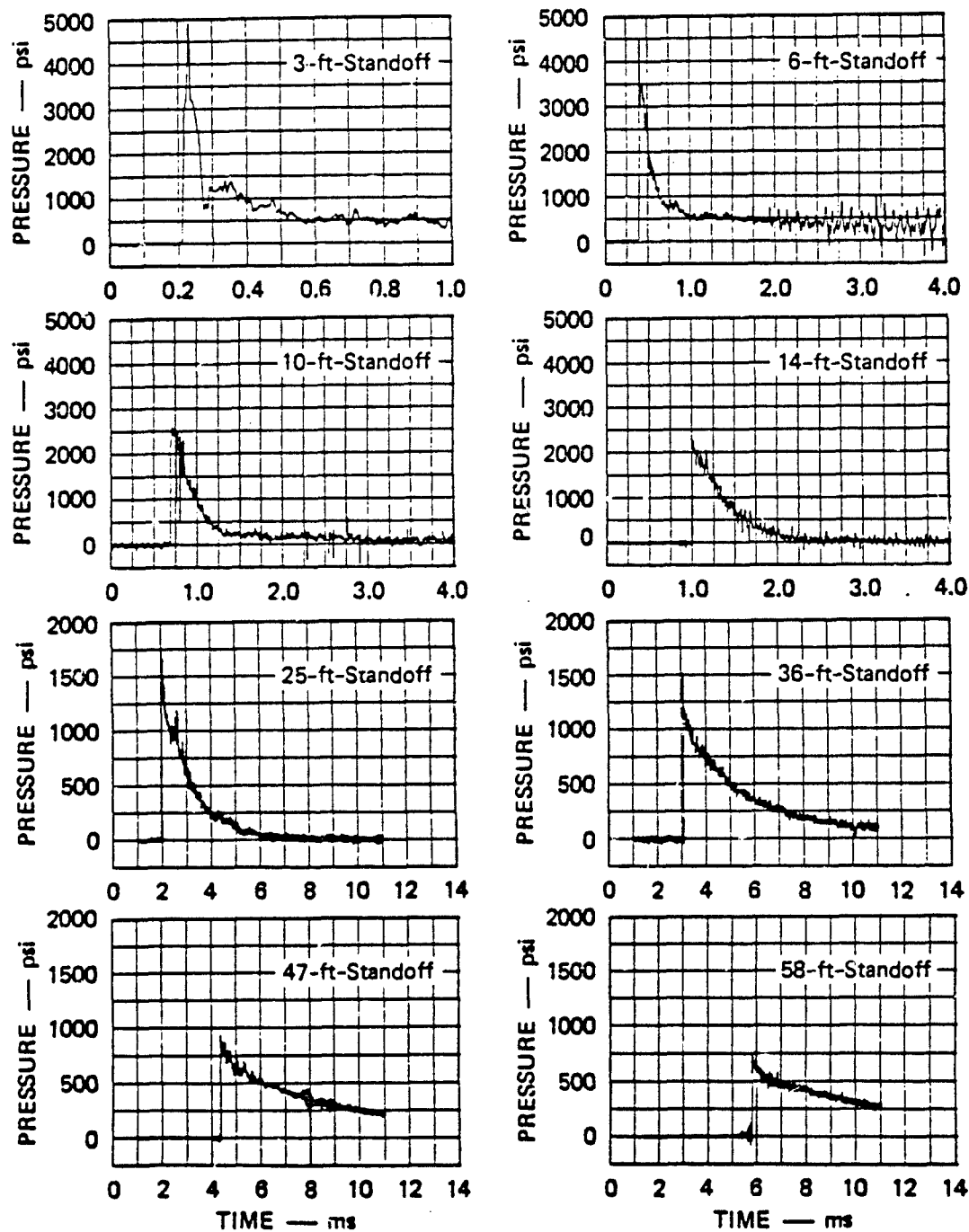
FIGURE 14   PRESSURE RECORDS FROM A SHOCK ATTENUATION TEST WITH STEEL PIPE

16

comparison between the calculated and measured peak pressures for the three tests with steel pipe is shown in Fig. 15.
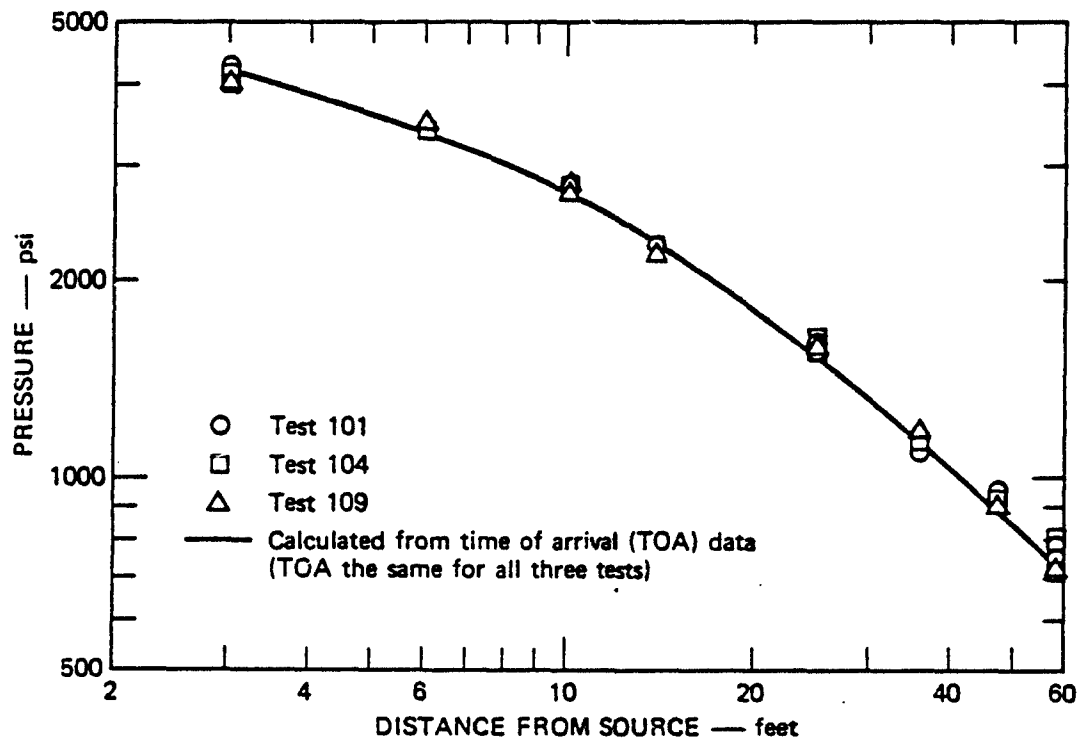

FIGURE 15   PEAK PRESSURE VERSUS DISTANCE FOR THE THREE SHOCK ATTENUATION
TESTS USING STEEL PIPE

A typical ionization probe record is shown in Fig. 16. The probe records showed that the start of the transition zone ranges from 0.2 ms behind the shock front and 14 ft from the source to 3.5 ms behind the shock front and 58 ft from the source. The probe records and the pressure records were used to construct a plot of TOA of the shock front and of the transition zone versus distance from the source. This plot is shown in Fig. 17.

17
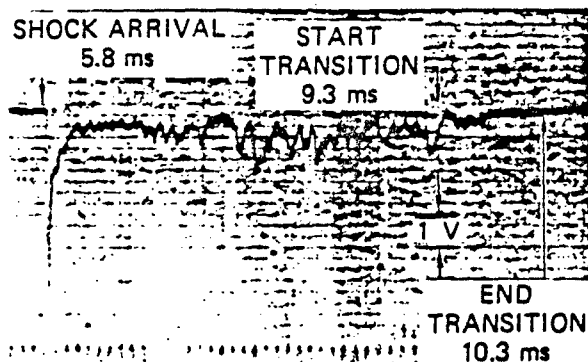
MP-7285-198

FIGURE 16 TYPICAL IONIZATION PROBE RECORD

(Test with steel pipe, 58-ft-standoff)
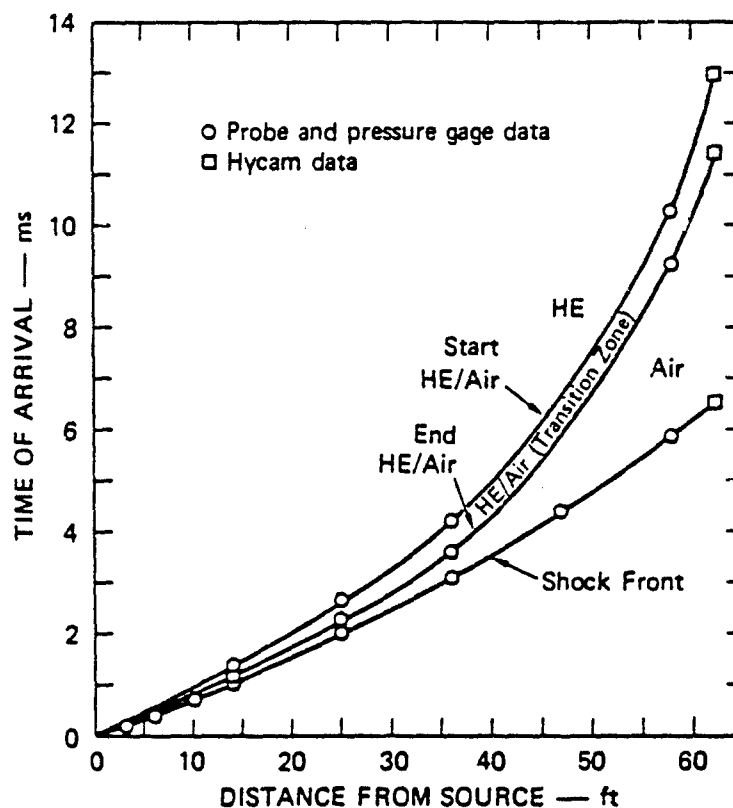
MA-7285-52

FIGURE 17 TOA (SHOCK AND POINT CONTACT) VERSUS DISTANCE
FROM SOURCE FROM TEST 109

1-inch-thick Comp B Charge.

Concrete Trench Experiments

Two tests were conducted with concrete trenches. In Test 116, the concrete trench was buried 12 to 15 in. deep, so the only added attenuation effect relative to the steel tube was trench expansion. In Test 117, the trench was buried 2.3 in. deep, a depth scaled from the baseline design. This test had the added effects of asymmetrical expansion and trench- to-surface venting.

The 60-ft-long concrete trenches were made up of 21 fiber-reinforced concrete trench sections, each with a 6-in.-ID, a 1-in.-thick wall, and a length between 30 and 36 in. The same concrete and fiber mix was used as in the short sections tested to study expansion and venting. The compressive strength ranged from 4100 psi to 8600 psi and averaged 6800 psi. The tensile splitting strength ranged from 800 psi to 1800 psi and averaged 1400 psi. In the field, the individual trench sections were joined together with epoxy. A laser was used for alignment.

The soil was obtained from the same location at the HAVE HOST site as used in the expansion and venting tests. It was backfilled into a 3-ft-wide, 3-ft-deep excavation. For Test 117, the laser was used to aid in leveling the soil surface to within ± 0.1 in. For both tests, the soil was backfilled in layers of 4 to 6 in. Each layer was compacted to a nominal 110 lb/ft^3 dry density at a water content of 3 to 5 percent using a mechanical, gasoline-engine-driven tamper. Actual dry densities measured ranged from 108 lb/ft^3 to 116 lb/ft^3, with an average of 111 lb/ft^3. Measured water contents ranged from 2.9 to 5.3 percent.

Radial displacement of the trench wall was measured with linear variable displacement transducers (LVDTs). The LVDT core was connected to the outer trench wall at the springline by a 2.5-in.-long push rod. Each LVDT body was backed up by a 1.5-in.-diameter, 6-in.-long steel slug located 6 in. from the trench wall. Thus, the slug remained stationary until the shock wave in the soil reached it (about 0.5 ms). Because of its mass, the slug moved only a short distance thereafter. These tests were also photographed with three high-speed cameras.

19

In both tests, the concrete trench fractured over the entire
60-ft length. For the deep-buried trench in Test 116, there was only
minor breakout, with most pieces still under the soil cover. In Test
117, with the shallow depth of burial, the roof of the concrete trench
was thrown into the air and pieces were lying to either side of the
trench axis. The trench below the springlines expanded radially 0.5 to
1.5 in., yet was roughly in its original orientation. The fracture
patterns for Tests 116 and 117 were similar. The predominant fracture
was longitudinal. Longitudinal cracks were from a few inches long to 4
or 5 ft. The majority of longitudinal cracks ran uninterrupted past the
trench joints. However, some trench joints failed, causing the longitu-
dinal crack to end at the joint. The trench fragments were smaller
closer to the driver, indicating that the number of cracks increases
with the pressure. The relation between pressure and number of cracks
was similar to that found in the expansion and venting tests on short
concrete trench sections. The high-speed movies showed that in Test
117, venting took place after the trench crown had displaced between
2.2 in. and 3.9 in. These displacements are higher than observed in the
short section expansion and venting tests, possibly because of the
thicker trench wall and the lower pressure at the time of venting.

Interpretation of Results

We then compared the shock attenuation for the three types of
tests: steel pipe, deeply buried concrete trench, and concrete trench
with scaled soil cover. Figure 18 shows a log-log plot for the peak
pressure versus distance for each type of test. The curves are the peak
pressures calculated from the TOA data. (As discussed earlier, these
curves agree with the discrete peak pressures measured in the tests.)
The pressure attenuation for the steel pipe, shown by the solid line, is
caused primarily by the finite thickness of the source and by frictional
drag on the pipe walls. The pressure attenuation for the deep-buried
concrete trench, shown by the upper dashed line, should be the same as
that of the steel pipe except for the effect of trench expansion.
Comparison of the solid and upper dashed lines show that the effect of

20

trench expansion was to decrease the peak pressure by 55 percent at 58 ft from the source.

The pressure attenuation for the concrete trench with the scaled soil cover, shown by the lower dashed line, should be the same as that of the deep-buried concrete trench except for the effects of asymmetrical expansion and trench-to-surface venting. Comparison of the dashed lines shows no difference in peak pressure for the first 40 ft of propagation and only a 15 percent decrease in peak pressure after a distance of 58 ft. In these data, the effect of asymmetrical expansion of the trench crown and the effect of venting cannot be separated; however, it is clear that the combined attenuation effects of asymmetric expansion and venting are minimal compared with the effect of simple expansion.

Average springline velocities over the first millisecond after shock arrival were determined from the LVDT records and are plotted in Fig. 19. The closeness of the data from the two tests suggests that for the range of pressures and trench lengths in the these tests, the attenuating effect of upstream asymmetric expansion and venting also has little or no affect on the impulse for up to 1 millisecond after shock arrival downstream.

Conclusions

The major conclusions from the expansion and venting tests are that

(1) Approximately symmetric longitudinal cracks form in the trench soon after shock arrival.

(2) After reflections from the free surface of the soil, the roof fragments and soil move vertically as a slug.

(3) Venting occurs directly above the roof when the bottom of the slug reaches the original soil surface.

The data from the shock attenuation tests showed consistently lower peak pressures as more attenuation mechanisms were introduced. For example, the effect of trench expansion (concrete trench versus steel pipe) was to decrease the peak pressure by 55 percent at an L/D of 116. For the test of a concrete trench with a scaled soil cover, the peak

21

Steel pipe
Concrete trench, deep buried
Concrete trench, scaled soil cover
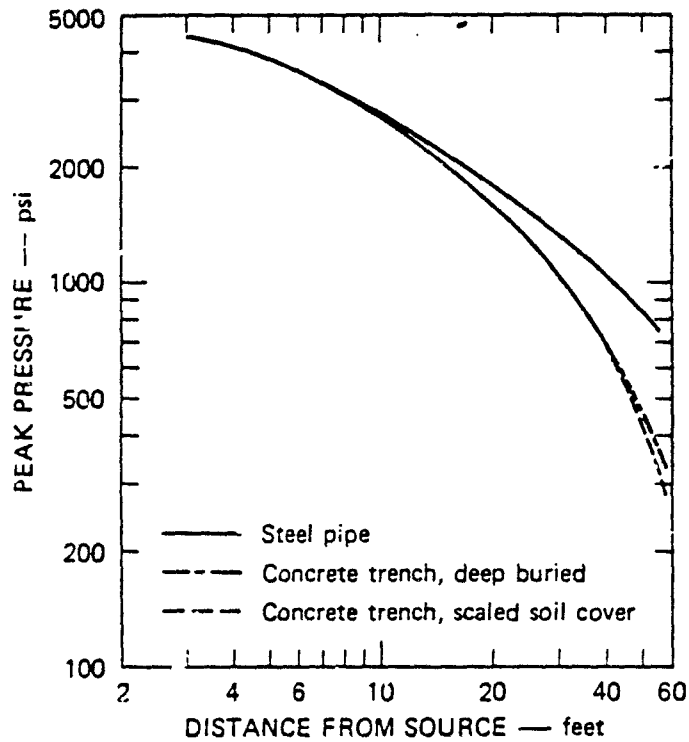
MA-7285-92A

FIGURE 18   COMPARISON OF PEAK PRESSURE VERSUS DISTANCE
FOR TEST 109 (STEEL PIPE), TEST 116 (CONCRETE
TRENCH, DEEP BURIED) AND TEST 117 (CONCRETE
TRENCH, SCALED SOIL COVER)
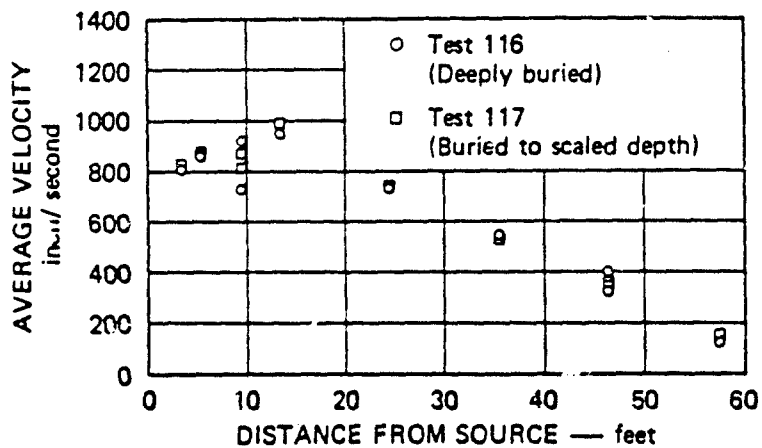
MA-7285-91A

FIGURE 19   AVERAGE SPRINGLINE VELOCITY VERSUS DISTANCE
FROM SOURCE

22

pressure was the same as that of the deep-buried concrete trench for the
first 40 ft (L/D = 80). Thus asymmetrical expansion of the trench and
venting has no effect on peak pressure up to L/D = 80 and has only a
small effect (15 percent decrease) on peak pressure at L/D = 116.

Acknowledgment

References

1. J. R. Bruce and J. K. Gran, "Laboratory Investigation of Expansion
    and Venting and Plug Response in the MX Trench," SRI International,
    Menlo Park, CA, Final Report DNA5235F (1 February 1979).

2. J. R. Bruce and J. K. Gran, "Laboratory Investigation of Shock
    Attenuation and Spur Response in the MX Trench," SRI International,
    Menlo Park, CA, Final Report DNA 5086F (28 February 1979).

3. Testing Engineers, Inc., Santa Clara, CA.

4. J. G. Jackson, Jr., Waterways Experiment Station, Vicksburg,
    Mississippi, "Recommended Calculational Properties for HAVE HOST
    High-Density Backfill," letter to AFWL, Kirtland AFB, New Mexico
    (7 July 1977); "Recommended Calculational Properties for HAVE HOST
    Low-Density Backfill," letter to AFWL, Kirtland AFB, New Mexico
    (5 April 1977).

5. L. Seaman, "SRI PUFF 3 Computer Code for Stress Wave Propagation,"
    prepared for Air Force Weapons Laboratory, Air Force Systems
    Command, Kirtland AFB, New Mexico, Technical Report No. AFWL-TR-70-
    51, Stanford Research Institute, Menlo Park, California (September
    1970).

6. S. J. Ayala, "HAVE HOST T-1 Quick Look," Preliminary Report
    prepared by AFWL/DEP for the Space and Missile Systems Organization
    (SAMSO), Project 627A, Program Element 6330F under DNA Contract.
    Subtask H35HAXSX355, Program Element 62710F (25 August 1977).